Butt, H.-J., Berger, R., Steffen, W., Vollmer, D., & Weber, S. A. L. (2018). Adaptive Wetting-Adaptation in Wetting. *Langmuir, 34*(38), 11292-11304. doi:10.1021/acs.langmuir.8b01783.

Adaptive Wetting-Adaptation in Wetting

Butt, H.-J., Berger, R., Steffen, W., Vollmer, D., & Weber, S. A. L.

https://doi.org/10.1021/acs.langmuir.8b01783

Adaptive wetting – adaptation in wetting

Hans-Jürgen Butt[1], Rüdiger Berger[1], Werner Steffen[1], Doris Vollmer[1], Stefan A.L. Weber[1,2]

[1] Max Planck Institute for Polymer Research, Ackermannweg 10, 55128 Mainz, Germany

[2] Johannes Gutenberg University, Department of Physics, Staudingerweg 10, 55128 Mainz, Germany

butt@mpip-mainz.mpg.de

Abstract

Many surfaces reversibly change their structure and interfacial energy upon being in contact with a liquid. Such surfaces adapt to the specific liquid. We propose a first order kinetic model to describe dynamic contact angles of such adaptive surfaces. The model is general and does not refer to a particular adaptation process. The aim of the proposed model is to provide a quantitative description of adaptive wetting and to link changes in contact angles to microscopic adaptation processes. By introducing exponentially relaxing interfacial energies and applying Young's equation locally, we predict a change of advancing Θ_a and receding contact angles Θ_r depending on the velocity of the contact line. Even for perfectly homogeneous and smooth surfaces, a dynamic contact angle hysteresis is obtained. As possible adaptations, we discuss changes and reconstruction of polymer surfaces or monolayers, diffusion and swelling, adsorption of surfactants, replacement of contaminants, reorientation of liquid molecules, or formation of an electric double-layer.

https://doi.org/10.1021/acs.langmuir.8b01783

Introduction

The dynamics of a liquid wetting a solid surface is a complex process because different length and time scales are involved [1, 2]. Even on an inert, rigid, smooth and homogeneous solid surface a quantitative description of wetting dynamics is still a challenge [3, 4, 5]. So far, models which describe the wetting dynamics of moving contact lines focused on thermally activated hopping processes or on hydrodynamic effects [6, 7, 8, 9]. The challenge becomes even bigger for adaptive or responsive surfaces, that is, surfaces which change their properties with external conditions such as temperature, humidity, electric and magnetic fields or the presence of the liquid itself [10, 11, 12, 13]. The aim of this manuscript is to introduce a model to describe wetting dynamics, focusing on temporal and spatial changes of the interfacial energies.

Here, we focus on a subclass of adaptive surfaces, in particular those that spontaneously change in the presence of the liquid or its vapor. We also consider that the liquid adapts to the presence of the interface with a solid or air. We do not consider surfaces which change with external conditions such as temperature, electric or magnetic fields etc. We do not take reactive, corrosive or soluble surfaces [14] into account, because chemical reactions or dissolution usually lead to multiple effects including topographic changes.

For clarity we give a few examples of solid surfaces which "adapt" in the presence of the liquid:

- **Polymer reconstruction**. Many polymer surfaces adapt to the surrounding medium [15, 16, 17, 18, 19, 20, 21, 22, 23, 24, 25, 26, 27, 28, 29, 30, 31]. They reconstruct due to a reorientation of side groups or a selective exposure of specific segments (Fig. 1A).
- **Diffusion and swelling**. Liquid can diffuse into the polymer [32, 33, 34] (Fig. 1B). For example, not only organic liquids [35] but also up to 30-40 mM of water are absorbed and diffuse into polydimethylsiloxane (PDMS) elastomers [36, 37, 38]. If the amount of liquid diffusing into the polymer is significant and polymer and liquid are partially miscible, the polymer will swell [39, 40, 41, 42, 43, 44]. Water, for example, swells polyethylene glycol (PEG) or polyelectrolyte brushes [45].
- **Mixed polymer brushes**. The composition of polymer surfaces with mixed polymers or polymer brushes changes depending on the type of fluid they are exposed to (Fig. 1C) [46, 47, 48, 49, 50, 51, 52, 53, 54, 55, 56]. The non-miscible polymer collapses and is hidden underneath the compatible polymer, which swells.
- **Recovery of PDMS**. PDMS, made hydrophilic e.g. by plasma treatment, electric discharge or contamination, is known to regain its hydrophobicity by exposure to air [57, 58, 59, 60, 61, 62]. Recovery is dominated by the diffusion of low-molecular weight oligomers from the bulk to the surface (Fig. 1D). Yokoyama et al. used this effect and deliberately added PDMS-*b*-PEG diblock copolymers to a PDMS matrix [63] (Fig. 1E). In air, the diblock copolymer was

https://doi.org/10.1021/acs.langmuir.8b01783

distributed in bulk PDMS. In water, the block copolymer diffused to the surface and the PEG chains were exposed making the surface hydrophilic [64].

- **Reconstruction of organic monolayers**. Some organic monolayers change their structure in water depending on temperature or pH or other liquids [65, 66, 67]. Another example for adaptive monolayers are end-functionalized alkane chains on a silicon wafer in hexadecane [68, 69] (Fig. 1F).
- **Replacement of contamination/adsorption layer**. As soon as a surface is exposed to air, water and airborne hydrocarbons adsorb. Such adsorbed layers have been studied for a number of surfaces, such as metals [70, 71], mica [72], graphite [73] and ceramic oxides [74]. When the surface is wetted, the adsorbed layer remains at the interface and can change its structure or be replaced (Fig. 1G).

In all these examples "air" can also be another gas or the vapor. It can also be a different liquid which is immiscible with the wetting liquid.

Also, in the liquid, molecules adapt to the presence of the solid and change their structure close to the interface:

- **Ordering of liquid molecules**. Hansen & Miotto [75] and later Elliott & Riddiford [76] realized that the liquid molecules form an ordered layer at the solid-liquid interface which is different from the molecular structure of the free liquid surface. Thus, the liquid "adapts" to the presence of the solid interface. Liquid molecules change their molecular order when wetting/dewetting a surface [75, 76, 77] (Fig. 1H).
- **Adsorption of surfactants**. Surface active molecules dissolved in the liquid adsorb to newly wetted solid surface at the advancing side and freshly created liquid surface at the rear of a moving drop (Fig. 1I) [3, 78, 79, 80]. Their structure and surface concentration depends on the specific interface.
- **Formation of electric double layer**. Ions from aqueous solution adsorb to a surface or dissociate from ionizable groups leading to surface charging (Fig. 1J). Electric double layers also form at the water-air interface. As one example, in figure 1J the solid surface is positively charged, as for Al_2O_3 in water at neutral pH, and the water-air interface is slightly negatively charged.

https://doi.org/10.1021/acs.langmuir.8b01783

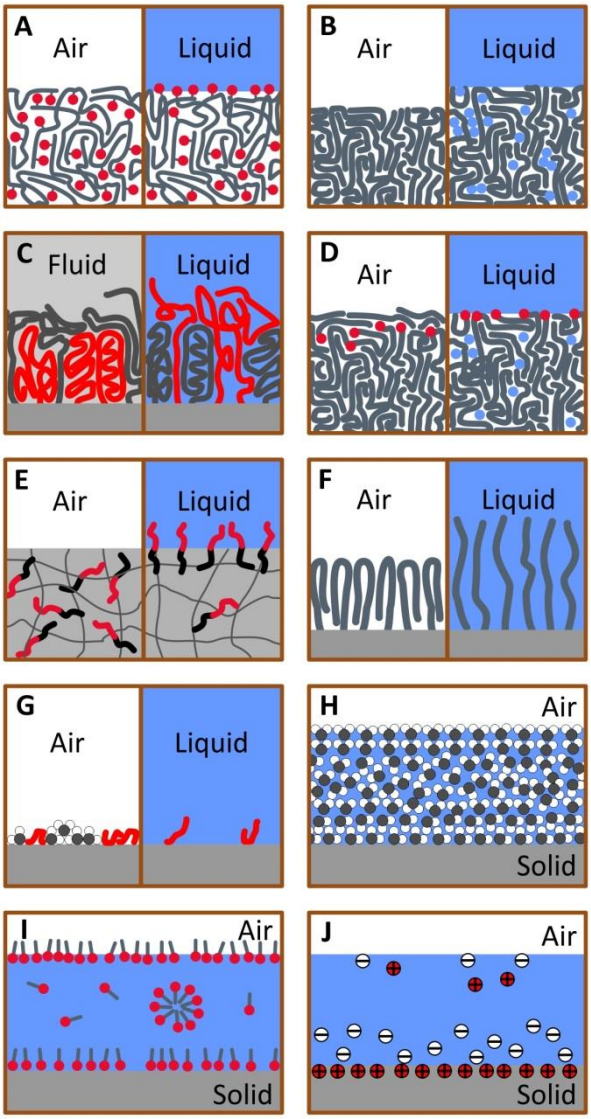

Figure 1. Schematic examples of surface adaptations. Air is drawn as white area. The same arguments hold if a second, immiscible liquid is used instead of air. (A) Reconstruction of a polymer surface by reorientation and rearrangement. Lyophilic side groups (red circles) tend to orient towards the liquid (B) Diffusion of liquid molecules (blue circles) into polymer and swelling. (C) Mixed polymer brush with chains which are either compatible with the liquid (red) or more compatible with another fluid (grey). (D) Recovery of polymer as in PDMS. Hydrophilic groups (red) covered in air by low-molecular weight components are exposed in water and water molecules (blue) diffuse into the polymer. (E) Block copolymer with a hydrophilic (red) and hydrophobic part (black) in an elastic organogel. (F) Reconstruction of an organic monolayer depending on environment. (G) Replacement of adsorbed molecules and contaminants. In this example water and organic molecules (red) are adsorbed in air. Water molecules (black circles with two attached white circles) are replaced by the liquid. The organic material is only partially replaced and changes its conformation. (H) Molecular ordering of liquid molecules at the solid-liquid and the liquid-air interfaces. (I) Surfactants

https://doi.org/10.1021/acs.langmuir.8b01783

binding to both interfaces. (J) In liquids with high dielectric permittivity, electric double layers form at interfaces.

Adaptation has two important consequences: It leads to contact angle hysteresis and changing dynamic contact angles.

Contact angle hysteresis: Wetting of a specific surface is in fact characterized by two contact angles: The advancing contact angle Θ_a measured just before a liquid front starts to advance, and the receding contact angle Θ_r, measured just before the liquid front recedes. The difference between the two, $\Theta_a - \Theta_r$, is called contact angle hysteresis. Without contact angle hysteresis drops would slide off any surface even at low tilt angles [81, 82, 83, 84, 85]. Contact angle hysteresis provides friction to moving drops [86, 87]. Contact angle hysteresis can be caused by several effects, e.g. surface roughness, heterogeneity, adsorption of contaminants at the contact line [1, 3]. Here we show that adaptation of the wetting surface is another reason for contact angle hysteresis.

Dynamic contact angles: Contact angles depend on the speed of the three-phase contact line v, here briefly called contact line. The dynamic advancing contact angle $\Theta_a(v)$ increases with wetting speed until it reaches 180° and air is entrapped. The dynamic receding contact angle $\Theta_r(v)$ decreases with dewetting speed until it becomes zero and a film is formed. Often, velocity dependent contact angles are described by the molecular kinetic theory (MKT) or hydrodynamic theory [3, 4, 5, 6, 7, 9]. MKT is based on thermally activated adsorption/desorption processes at an advancing/receding liquid front. Hydrodynamic and MKT theory describe velocity dependent contact angles. For many practical cases, in particular for low velocities, hydrodynamics is not sufficient, and MKT leads to fitting parameters which do not reflect the underlying physical process. Here, we suggest that adaptation also changes the dynamic contact angles. For simplicity we ignore changes in the contact angle due to e.g. hydrodynamics or thermally activated processes. Combining several effects, e.g. hydrodynamics with adaptation, is beyond the scope of this paper.

We propose a simple model based on Young's equation which takes into account adaptation of surfaces and interfaces. Strictly, Young's equation is only valid in equilibrium. Even interfacial tensions are only defined in equilibrium. In order to describe a moving contact line and thus an out-of-equilibrium situation, we apply Young's equation locally and we define local interfacial energies. The goals of our adaptation model are

- to derive a quantitative description of dynamic contact angles,
- to link contact angle dynamics to relaxation processes at interfaces,
- to suggest adaptation of the solid surface as one explanation for the observed changes in contact angle even at very low speeds of the contact line [88] and
- to suggest adaptation as an explanation for contact angle hysteresis even on smooth, homogeneous surfaces.

https://doi.org/10.1021/acs.langmuir.8b01783

Some adaptive surfaces change their topography or become soft when getting into contact with a liquid and thus change the wetting properties. One example is swelling polymer surfaces. These additional effects may even dominate. However, they are not within the scope of this manuscript.

Theory

Adaptation model for interfacial energies

We consider a smooth, homogeneous, undeformable, and inert planar solid surface. In air or vapor its equilibrium surface energy is γ_S^∞. When it gets into contact with a liquid for example when placing a drop on a surface (Fig. 2A) or when a drop advances (Fig. 2B), the composition and structure of the surface changes. The surface may reorganize, swell, ions may dissociate or bind, adsorbed molecules and contaminants get dissolved or adsorb to the surface. All these processes take time. As a result, the energy of the solid-liquid interface changes from an initial value just after contacting the liquid γ_{SL}^0 to a new equilibrium value γ_{SL}^∞. γ_{SL}^∞ is reached when all these processes have relaxed to equilibrium. Due to the time dependence of the surface tension, we distinguish between the initial interfacial tensions (denoted by the superscript "0") and the equilibrium interfacial tensions, reached after a long time (denoted by the superscript "∞"). Here, we assume that the initial interfacial tension is higher than the equilibrium interfacial tension because the relaxation is spontaneous. Therefore, $\gamma_{SL}^\infty = \gamma_{SL}^0 - \Delta\gamma_{SL}$, where $\Delta\gamma_{SL}$ is positive.

In general, the change of the interfacial tension $\gamma_{SL}(t)$ from γ_{SL}^0 to γ_{SL}^∞ can be complex and will depend on the specific process considered. For simplicity we assume first order kinetics so that the interfacial tension relaxes exponentially:

$$\gamma_{SL}(t) = \gamma_{SL}^\infty + \Delta\gamma_{SL} e^{-t/\tau_{SL}} \qquad (1)$$

Here, τ_{SL} characterizes the relaxation time corresponding to the adaption of the solid-liquid interface.

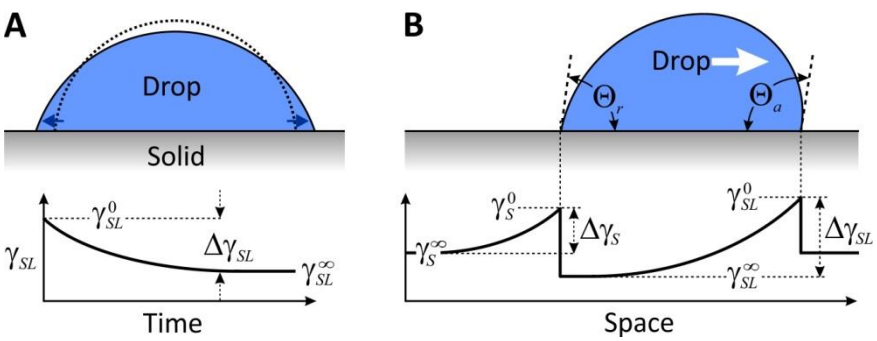

https://doi.org/10.1021/acs.langmuir.8b01783

Figure 2. Schematic of a spreading and a moving drop. (A) Sessile drop spreading on a surface after being placed. At the bottom the decrease of the interfacial tension $\gamma_{SL}(t)$ after the drop has been placed on the surface is sketched. γ_{SL}^0: interfacial tension just after placing the drop. γ_{SL}^∞: equilibrium value. (B) For a drop moving in steady state over a surface the development of the interfacial tension leads to a position-dependent interfacial tension.

There are exceptional cases, where $\Delta\gamma_{SL}$ is negative. Such cases of autophobic dewetting have been described for some liquid-solid combinations [89, 90, 91]. One example is cetyltrimethylammonium bromide (CTAB) dissolved in water on silica; at low concentration CTAB adsorbs spontaneously, creating a hydrophobic surface. Still, the free energy of adsorption then needs to be so high that in total the process is spontaneous. For simplicity we assume that $\Delta\gamma_{SL}$ is positive; the formalism can easily be applied also to negative $\Delta\gamma_{SL}$.

The same formalism is applied to describe processes when the liquid recedes and the solid is exposed to air again. Right after the liquid is gone, the surface energy of the solid-air interface is γ_S^0. Assuming reversibility, it relaxes back to γ_S^∞. Assuming again first order kinetics, the relaxation process can be described by

$$\gamma_S(t) = \gamma_S^\infty + \Delta\gamma_S e^{-t/\tau_S} \qquad (2)$$

Here, $\Delta\gamma_S$ is positive since the process is spontaneous. In particular, $\gamma_S^0 = \gamma_S^\infty + \Delta\gamma_S$. The relaxation time for the adaption of free solid surface, τ_S, will in general be different from τ_{SL} because the underlying processes occur in different environments.

At the receding side, free liquid surface is created as well. With respect to molecular ordering this process is usually fast. If, however, we also take into account adsorption processes, the surface tension of the free liquid surface will change behind the receding contact line. Assuming that the freshly created free liquid surface has an initial surface tension γ_L^0 which relaxes back to γ_L^∞ with a first order kinetics we have an additional time constant τ_L involved:

$$\gamma_L(t) = \gamma_L^\infty + \Delta\gamma_L e^{-t/\tau_L} \qquad (3)$$

Contact angle

The contact angles are given by a balance of forces at the three-phase contact line, which leads to the Young equation. In equilibrium, that is after adaptation, Young's equation is

$$\gamma_L^\infty \cos\Theta^\infty = \gamma_S^\infty - \gamma_{SL}^\infty \qquad (4)$$

https://doi.org/10.1021/acs.langmuir.8b01783

Here, Θ^{∞} is the contact angle in thermodynamic equilibrium. For $\gamma_{SL}^{\infty} < \gamma_{S}^{\infty}$, the contact angle Θ^{∞} is below 90°, as observed for lyophilic surfaces. For $\gamma_{SL}^{\infty} > \gamma_{S}^{\infty}$, as for example for water on fluorinated hydrocarbons, Θ^{∞} > 90°. For $\gamma_{SL}^{\infty} = \gamma_{S}^{\infty}$ the equilibrium contact angle is 90°.

For sessile drops the fact that the interfacial tension adapts has two consequences. First, when placing a liquid drop on an adaptive surface, its initial contact angle is higher than Θ^{∞} (Fig. 2A). Then the liquid will spread with a typical relaxation time τ_{SL}. Second, for a moving drop the dynamic contact angles at the front and rear will depend on the velocity (Fig. 2B).

Dynamic advancing contact angle

Let us consider an advancing liquid front on a solid (Fig. 2B). Since the interfacial energy behind the liquid front changes, the question arises: Which interfacial energy has to be inserted in Young's equation? Which length scale determines the contact angle? When the liquid front moves very slowly the interface behind the contact line has time to relax and the interfacial energy will be equal to γ_{SL}^{∞}. When the liquid front is fast the interface has no time to change and the relevant interfacial energy is γ_{SL}^{0}. In between, the interfacial tension gradually changes. In Young's equation we have to insert the interfacial tensions in the region of the contact line. In accordance with Hansen & Miotto [75] we call this region "peripheral thickness". Here, the peripheral thickness l_{SL} is the width of contact region, which influences the contact angle.

Here, we can only speculate about the width of the peripheral thickness. First, surface forces influence the shape of the liquid surface close to the contact line [92]. In this "core" [93] or "transition" [94] region the microscopic contact angle can be different from the macroscopic contact angle considered by Young's equation. The peripheral thickness should at least be as large as the range of surfaces forces. Typically surface forces range up to several 10 nm. Second, the solid surface experiences a surface stress. For a sessile drop, surface stress in the solid compensates for the vertical force exerted by the liquid surface tension [95]. Molecular dynamics simulations indicate that the solid region experiencing stress extends over ≈10 nm [96, 97, 98]. Third, one can consider the extent of an interface as a measure for the peripheral thickness. The extent of an interface is the region over which the surface structure is different than the bulk. In the liquid the region ranges from few molecular layers up to many nanometers, considering e.g. the electric double layer. Thus, the peripheral thickness depends on the specific nature of the interface. In the following we use 10 nm as a guess for the peripheral thickness.

Depending on the actual velocity of the contact line v the advancing contact angle is going to change:

https://doi.org/10.1021/acs.langmuir.8b01783

$$\cos\Theta_a = \frac{\gamma_S^\infty - \gamma_{SL}(t = l_{SL}/v)}{\gamma_L^\infty} = \cos\Theta^\infty - \frac{\Delta\gamma_{SL}}{\gamma_L^\infty} e^{-l_{SL}/v\tau_{SL}} \quad (5)$$

Thus, a relaxation process at the advancing contact line would lead to a velocity dependent contact angle. For a fast-moving contact line, $v \gg l_{SL}/\tau_{SL}$, the advancing contact angle is $\cos\Theta_a = \cos\Theta^\infty - \Delta\gamma_{SL}/\gamma_L^\infty$. As the wetting velocity decreases, the contact angle approaches the equilibrium value $\Theta_a \to \Theta^\infty$ for $v \ll l_{SL}/\tau_{SL}$. The relevant parameter is the ratio of the peripheral thickness, l_{SL}, and the relaxation time τ_{SL}. We define $v_{SL} \equiv l_{SL}/\tau_{SL}$ as the "adaptation velocity". The adaptation velocity is the independent new parameter in the theory; the peripheral thickness and the relaxation time always occur as l_{SL}/τ_{SL}.

As one example, the increase of the advancing contact angle is shown in Figure 3A for water and with γ_L^∞ =0.072 N/m, γ_S^∞ =0.06 N/m, γ_{SL}^∞ =0.04 N/m and $\Delta\gamma_{SL}$ =0.01 N/m. In the given example with l_{SL} = 10 nm and τ_{SL} = 0.1 – 100 µs, the adaptation velocity ranges from 0.1 mm/s to 0.1 m/s. At low velocity ($v \ll v_{SL}$) the adaptation process occurring over the peripheral thickness at the front, l_{SL}, still has time to proceed and the interfacial tension γ_{SL} reaches its equilibrium value γ_{SL}^∞. As a result, the equilibrium contact angle of Θ^∞=73.9° is reached. Then the advancing contact angles increase monotonically with increasing speed. At high velocity ($v >> v_{SL}$) the contact line moves so fast over a distance l_{SL} that the interfacial energy has not time to adapt. The interfacial energy entering Young's equation is γ_{SL}^0 rather than γ_{SL}^∞. In the specific example of Figure 3A this leads to a contact angle of 82.0°.

https://doi.org/10.1021/acs.langmuir.8b01783

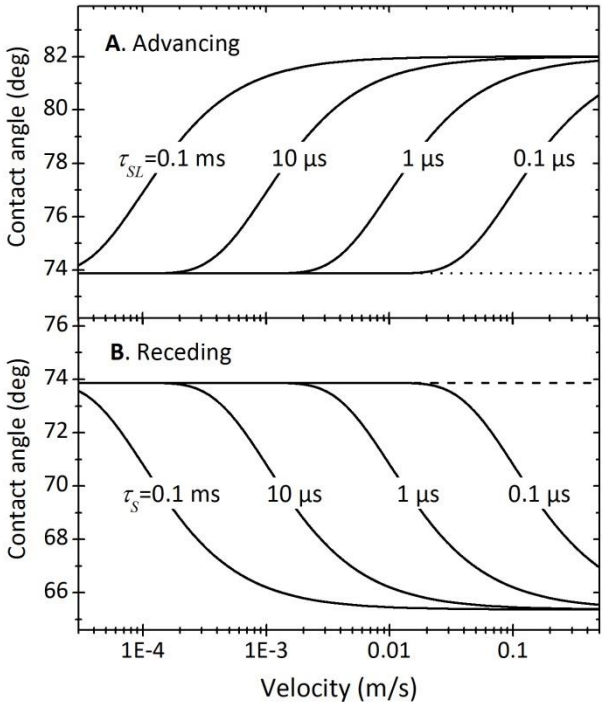

Figure 3: Dynamic advancing (A) and receding (B) contact angles for water (γ_L^∞=0.072 N/m) versus velocity of the contact line for different relaxation times. Contact angles were calculated with eqs. (5) and (8) inserting $\gamma_S^\infty = 0.06$ N/m, $\gamma_{SL}^\infty = 0.04$ N/m, $\Delta\gamma_S = \Delta\gamma_{SL} = 0.01$ N/m, and $l_{SL} = l_S = 10$ nm.

To move the advancing contact line at velocity v requires a force per unit length

$$f_a(v) = \gamma_L^\infty \left(\cos\Theta^\infty - \cos\Theta_a\right) = \Delta\gamma_{SL} e^{-v_{SL}/v} \qquad (6)$$

The energy dissipated per unit length of contact line and per time is $p_a = v f_a = v\Delta\gamma_{SL} e^{-v_{SL}/v}$. For a slowly moving contact line the molecules adapt to the new liquid environment even within the peripheral thickness; $p_a \to 0$ for $v_{SL} >> v$. The contact line therefore does not need to move up against a strong change in surface energy. Adaptation happening within the peripheral thickness contributes to a further spreading of the contact line. In contrast, for a fast moving contact line the molecules adapt far behind the contact line and the energy is dissipated as heat.

Spreading of a drop

When placing a drop of liquid onto an adaptive surface, the initial contact angle is given by $\cos\Theta_a = \left(\gamma_S^\infty - \gamma_{SL}^0\right)/\gamma_L^\infty$. Afterwards, the contact angle decreases towards Θ^∞ according to Eq. (5) with a time constant τ_{SL}. As a result, the contact radius a increases and the drop spreads (Fig. 4). From the spreading kinetics one can directly infer the relaxation time of the

https://doi.org/10.1021/acs.langmuir.8b01783

underlying process. Therefore, if one can devise an experiment where contact angle hysteresis due to inhomogeneity or roughness etc. can be neglected, the spreading kinetics directly reflects the adaptation kinetics.

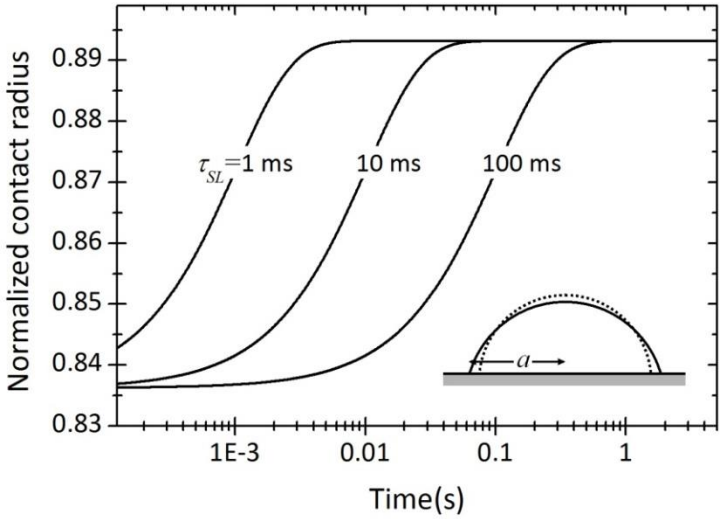

Figure 4: Normalized contact radius of a water drop (γ_L^∞=0.072 N/m) for different relaxation times τ_{SL}. We neglected gravity and assumed that the drop assumes the shape of a spherical cap. As the normalized contact radius we plot $a/V^{1/3} = \sin\Theta_a \left[\pi\left(1-\cos\Theta_a\right)^2\left(2+\cos\Theta_a\right)/3\right]^{-1/3}$. Here, a is the contact radius and V is the drop volume. The advancing contact angles were calculated with Eq. (5) inserting $\gamma_S^\infty = 0.06$ N/m, $\gamma_{SL}^\infty = 0.04$ N/m, and $\Delta\gamma_{SL} = 0.01$ N/m.

Dynamic receding contact angle

For a receding liquid, we have a similar effect as on the advancing side and we can treat the receding side in a similar way. We assume that the liquid had been in contact with the solid for a long time so that initially $\gamma_S(t=0) = \gamma_S^0$. Again, assuming a balance of interfacial energies to determine the contact angle we obtain:

$$\cos\Theta_r = \frac{\gamma_S(t = l_S/v) - \gamma_{SL}^\infty}{\gamma_L(t = l_S/v)} = \frac{\gamma_S^\infty + \Delta\gamma_S e^{-l_S/v\tau_S} - \gamma_{SL}^\infty}{\gamma_L^\infty + \Delta\gamma_L e^{-l_S/v\tau_L}} \qquad (7)$$

Since relaxation processes at the receding side are different from processes on the advancing side, we use a different peripheral thickness l_S and relaxation time τ_S. For simplicity we assume that the liquid surface tension reaches its equilibrium fast. Assuming the free liquid has reached equilibrium, $\Delta\gamma_L e^{-l_S/v\tau_L}$ can be neglected and Eq. (7) simplifies:

$$\cos\Theta_r = \cos\Theta^\infty + \frac{\Delta\gamma_S}{\gamma_L^\infty} e^{-l_S/v\tau_S} \qquad (8)$$

https://doi.org/10.1021/acs.langmuir.8b01783

Thus, on the receding side the contact angle is reduced. The characteristic adaptation velocity of the free solid surface is $v_S \equiv l_S/\tau_S$.

The receding contact angle decreases monotonically with increasing velocity (Fig. 3B). At low velocity the adaptation process occurring over the peripheral thickness still has time to complete and the surface tension γ_S reaches its equilibrium value γ_S^∞. At high velocity with no significant adaptation, the interfacial energy entering Young's equation is γ_{SL}^0 rather than γ_{SL}^∞. Applying the same example as for the advancing side (Fig. 3A) leads to a contact angle of 65.4° for high velocities. The transition is at the adaptation velocity, $v = v_S$. The force required to move a receding contact line is $f_r(v) = \Delta\gamma_S e^{-v_S/v}$ leading to a dissipated energy per time and unit length of $p_r = v\Delta\gamma_S e^{-v_S/v}$.

As a result of the increasing advancing and decreasing receding contact angles, contact angle hysteresis, $\Theta_a - \Theta_r$, increases with increasing velocity.

Moving drop

When a drop is moving over a surface, for example on a tilted plane, we need to consider the advancing and receding process. For simplicity we only consider a two-dimensional drop shaped like a cylinder. For a drop of length L the solid will be in liquid environment for a time $t_d = L/v$. At the front the contact angle is described by Eq. (5). For the receding side, we have to consider that the interfacial tension may still be higher than γ_{SL}^∞. To link the solid surface energy to the time it had been exposed to the liquid, we assume a two-state model. In the two-state model the surface molecules are either in a dry state or they are in a wet state. There is no "grey" state in between. The transition between the two states happens via first order kinetics. Thus after a time t_d the proportion of surface area still being in the "dry" state is $e^{-L/v\tau_{SL}}$, while the proportion of the surface being in the "wet" state is $1 - e^{-L/v\tau_{SL}}$. The surface energy of the solid state right after the drop has passed is thus $\gamma_S(t_d) = \gamma_S^\infty + \Delta\gamma_S e^{-v_S/v}\left(1 - e^{-L/v\tau_{SL}}\right)$. Using Young's equation again together with Eq. (8), we obtain a receding contact angle

$$\cos\Theta_r = \cos\Theta^\infty + \frac{\Delta\gamma_S}{\gamma_L^\infty} e^{-v_S/v}\left(1 - e^{-L/v\tau_{SL}}\right) - \frac{\Delta\gamma_{SL}}{\gamma_L^\infty} e^{-L/v\tau_{SL}} \qquad (9)$$

Three regimes can be distinguished (Fig. 5). They differ in the surface tensions and interfacial energies effective in Young's equation:

- Low velocity ($v \ll v_S$, Fig. 5A): All surface and interfacial tension are at their equilibrium values. $\gamma_S = \gamma_S^\infty$, $\gamma_{SL} = \gamma_{SL}^\infty$, $\gamma_L = \gamma_L^\infty$. As a result $\Theta_r = \Theta^\infty$.

https://doi.org/10.1021/acs.langmuir.8b01783

- Intermediate velocity (v_S << v << L/τ_{SL}, Fig. 5B): The solid-vapor surface has no time to relax so that $\gamma_S = \gamma_S^0$. The interfacial tension has time to equilibrate and $\gamma_{SL} = \gamma_{SL}^\infty$. As a result $\gamma_L^\infty \cos\Theta_r \approx \gamma_S^0 - \gamma_{SL}^\infty$.
- High velocity (L/τ_{SL} << v, Fig. 5C): The solid-liquid interfacial energy has not time to equilibrate. As a result, $e^{-L/v\tau_{SL}} \to 1$ and the second term in Eq. (9) vanishes. The rear contact line of the drop passes a surface which is still in the dry state. Then, $\gamma_S \to \gamma_S^\infty$ and $\gamma_L^\infty \cos\Theta_r \to \gamma_S^\infty - \gamma_{SL}^0$.

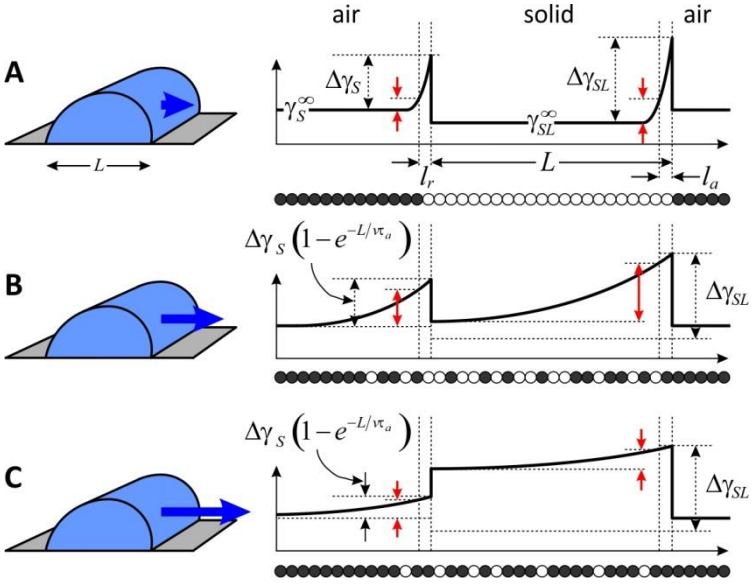

Figure 5: Interfacial energies for a two-dimensional drop moving at low (A), intermediate (B) and high (C) speed. The two red arrows indicate the energy dissipated per unit length. The white and black circles underneath the drop indicate a typical set of surface molecules to be either in the wet (open circles) or dry (filled circles) state, respectively. In this figure we assumed that $\gamma_S^\infty > \gamma_{SL}^\infty$.

To demonstrate the effect, we calculated the receding contact angle for a water drop of 2 mm length moving at different velocities (Fig. 6). The parameters used in the example were the same as in Figure 3. For simplicity we assumed that the adaptation process at the solid-liquid and solid-air interfaces are equally fast, $\tau_{SL} = \tau_S$. The curve plotted for τ_S = 0.1 ms is similar to the curve in Figure 2B: The contact angle monotonically decreases from its equilibrium value Θ^∞=73.9° to 65.4°. For τ_S = 1 ms both adaptation processes are effective. As a result of the increasing effective surface tension of the solid the contact angle decreases around v = 0.1 mm/s. At v > 1 m/s it starts to increase again, caused by the increasing energy of the solid-liquid interface. For τ_S = 1 ms the decrease of the contact angle is almost complete even at a velocity as low as 10 µm/s. Therefore the increase around v=0.2 m/s is clearly visible. For τ_S = 0.1 s even at very low velocities the adaptation at the rear of the drop

https://doi.org/10.1021/acs.langmuir.8b01783

is not effective and the adaption of the solid-liquid interface already becomes effective at v=2 cm/s.

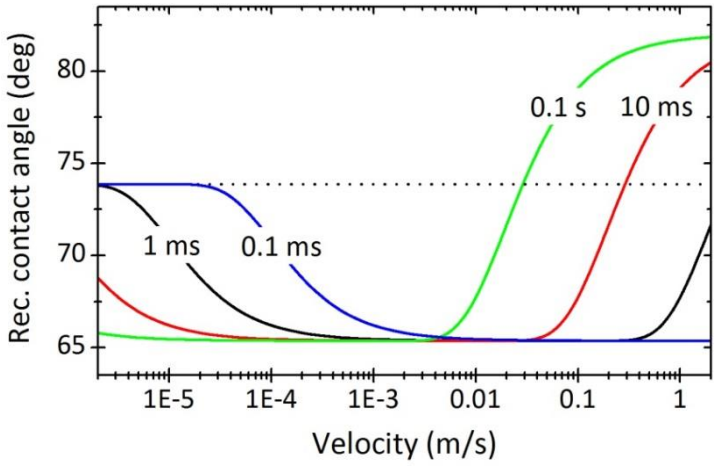

Figure 6: Dynamic contact angle at the rear of a moving two-dimensional drop (cylindrical shape moving perpendicular to the axis of the cylinder) versus velocity. Contact angles were calculated with Eq. (9) and γ_L=0.072 N/m, a length of L=2 mm, $\gamma_S^\infty = 0.06$ N/m, $\gamma_{SL}^\infty = 0.04$ N/m, $\Delta\gamma_S = \Delta\gamma_{SL} = 0.01$ N/m, and $l_S = 10$ nm.

Experimentally it will be challenging to observe both adaptation processes with a moving drop. Reason: The contact radius of the drop is much larger than the peripheral thicknesses, L >> l_{SL},l_S. Therefore, the two adaptation times allowed for a relaxation $l_{SL}/v \approx l_S/v$ and L/v are well separated. Covering both time scales in one experiment is difficult.

Energy dissipation

For simplicity we consider again a two-dimensional drop. For a two-dimensional moving drop the force per unit length is

$$\begin{aligned} f_d &= \gamma_L^\infty \left(\cos\Theta_r - \cos\Theta_a\right) \\ &= \gamma_L^\infty \left[\cos\Theta^\infty + \frac{\Delta\gamma_S}{\gamma_L^\infty} e^{-v_S/v}\left(1 - e^{-L/v\tau_{SL}}\right) - \frac{\Delta\gamma_{SL}}{\gamma_L^\infty} e^{-L/v\tau_{SL}} - \cos\Theta^\infty + \frac{\Delta\gamma_{SL}}{\gamma_L^\infty} e^{-v_{SL}/v}\right] \\ &= \Delta\gamma_S e^{-v_S/v}\left(1 - e^{-L/v\tau_{SL}}\right) + \Delta\gamma_{SL}\left(e^{-v_{SL}/v} - e^{-L/v\tau_{SL}}\right) \end{aligned} \quad (10)$$

This equation leads to

$$p_d = v\Delta\gamma_S e^{-v_S/v}\left(1 - e^{-L/v\tau_{SL}}\right) + v\Delta\gamma_{SL}\left(e^{-v_{SL}/v} - e^{-L/v\tau_{SL}}\right) \quad (11)$$

for the energy dissipated per unit time and unit length of contact line. It is again instructive to distinguish three velocity regimes:

https://doi.org/10.1021/acs.langmuir.8b01783

- Low velocity (v << v_S,v_{SL}, Fig. 5A): $p_d \to 0$ Equilibrium is reached within the advancing and receding peripheral thickness. As a result, not much energy is dissipated by adaptation.
- Intermediate velocity (v_S,v_{SL}<<v<<L/τ_{SL}, Fig. 5B): $p_d \approx v\Delta\gamma_S\left(1-e^{-L/v\tau_{SL}}\right)+v\Delta\gamma_{SL}\left(1-e^{-L/v\tau_{SL}}\right)$ $=v\left(\Delta\gamma_S+\Delta\gamma_{SL}\right)\left(1-e^{-L/v\tau_{SL}}\right)$. If the drop is short, not much energy is dissipated. The drop has passed before the molecules could adapt. If the drop is long, maximal energy is dissipated. The adaptation happens underneath the drop but only negligibly in the peripheral zone. All the energy is dissipated as heat.
- High velocity (L/τ_{SL}<<v, Fig. 5C): Neither the solid-air nor the solid-liquid interfacial tension had time to equilibrate. $p_d \to 0$.

Discussion

One aim of the proposed model is to provide a framework for a discussion of adaptive wetting and focus the discussion to relevant questions. One of the questions is: What is the peripheral thickness and how does it depend on the materials and liquid? Another question is: Which processes are relevant? What are the structural changes? On which time scale and with which kinetics do they occur? A prerequisite for adaption to have an effect is that the relaxation times are slow enough compared to the time of the advancing/receding contact line to pass the peripheral thickness.

Relaxation times

Therefore, here we address the last question and give first estimates of time constants from the literature (Fig. 7). We consider processes at the advancing and the receding front both at the solid and the liquid side. We did not find quantitative experimental relaxation times with respect to the reconstruction of organic monolayers and the replacement of contaminants or adsorption layers.

Polymer reconstruction. Time required for the reconstruction of polymer surfaces are usually reported to be in the range of few seconds up to days [19, 20, 22, 27, 28, 29, 47]. Much faster relaxation processes may be involved but are difficult to detect and it is possible that nobody was searching for them.

Diffusion and swelling. Diffusion of liquid molecules into the polymer or even swelling may occur when a polymer gets into contact with a liquid. The associated relaxation time is connected to the diffusion constant D by

$$\tau_d = \frac{\Delta z^2}{D} \qquad (12)$$

https://doi.org/10.1021/acs.langmuir.8b01783

Here, Δz is the depth determining the wetting properties of a surface. To estimate relaxation times for a typical example, namely water diffusing into PDMS (D=2×10^{-9} m^2/s [36, 37]), we assume that once the first 100 nm have been penetrated the interfacial tension is roughly at its equilibrium value. With Δz=100 nm the relaxation time will be of the order of 5 µs. Three more examples: Water diffusing into a plasma-polymerized polynorbornene film with D=1.4×10^{-13} m^2/s [34] leads to $\tau_{SL} = \tau_d \approx$ 70 ms. For polyamides D=4.6×10^{-13} m^2/s was reported for the diffusion of water molecules leading to $\tau_d \approx$ 22 ms [99]. From the increases in weight of toluene diffusing into a crosslinked polystyrene sphere, a diffusion coefficient of $D \approx R^2/\tau$ can be estimated; R is the radius of the sphere, τ the time to reach equilibrium swelling. Taking the results of measurements of Zhang et al. [39] we estimate $D \approx 4\times10^{-12}$ m^2/s leading to $\tau_d \approx$ 3 ms.

Swelling of a polymer gel is a complex process because diffusion, transport of liquid, and deformation of the gel are coupled and the diffusion constant depends on the degree of swelling [40, 100, 101, 102, 103]. In swelling experiments, typically the gain in weight is measured after immersing an initially dry, macroscopic piece of gel in liquid. Such curves are recorded over many minutes. For hydrogels, effective diffusion constants for water have been obtained by extrapolating the weight-versus-time curves to the initial phase and fitting them with pseudo second order kinetics [43, 44, 45, 102, 104]. Resulting diffusion coefficients range from 4×10^{-12} m^2/s up to the self-diffusion coefficient of water at 25°C of 2.3×10^{-9} m^2/s. Assuming that a penetration of 100 nm is sufficient, we expect that typical relaxation time are faster than 3 ms.

Mixed polymer brushes. The few systematic studies of adaptation of polymer brushes report typical relaxation times of the order of 1-100 min [105, 106].

Recovery of PDMS. The recovery of the hydrophobicity of PDMS after exposing it to a plasma, when being contaminated, or otherwise treated is dominated by the diffusion of low-molecular weight oligomers from the bulk to the surface. Relaxation times between 5 min up to several days have been reported. [59, 60, 61, 62, 107]. The relaxation process can in principal be described by diffusion theory [62, 64, 108]. However, the concentration and diffusivity of the low-molecular weight components are usually not known.

Orientation and molecular arrangement of liquid molecules at interfaces. To estimate the time for the relaxation of molecular structure of a liquid, we take the time required for a molecule to diffuse its own diameter. With the self-diffusion coefficient D and the molecular radius R the relaxation time for liquid ordering would be $\tau_{LO} = (2R)^2/6D$. The diffusion coefficient can be estimated from the viscosity η by:

$$D = \frac{k_B T}{6\pi\eta R} \qquad (13)$$

https://doi.org/10.1021/acs.langmuir.8b01783

Here, the diffusion coefficient is related to the hydrodynamic radius of the molecule R by Stokes equation. k_B is Boltzmann's constant and T is the absolute temperature. Estimating the radius of a molecule with molar mass M_W from its density ρ and the Avogadro constant N_A, gives us $R \approx \left(M_W / 8 N_A \rho\right)^{1/3}$. The time for molecular arrangement is then roughly

$$\tau_{LO} = \frac{\pi \eta M_W}{2 N_A \rho k_B T} \tag{14}$$

Relaxation times estimated with Eq. (14) range from ≈10 ps for water [109, 110, 111, 112] to nanoseconds for octamethylcyclotetrasiloxane (OMCTS) or glycerol.

At interfaces the relaxation process can be different from reordering in bulk. Often, the reorientation dynamics at a liquid-vapor interfaces is slightly faster than in the bulk while at liquid-solid interfaces it is slightly slower than in the bulk [113]. For many liquids, the assumption of fast equilibration cannot be made. For example, methanol and in particular ethanol molecules show long residence times on a silica surface with lifetimes of hydrogen bonds of 1-20 ns [114]. The relaxation dynamics of ionic liquids at metal electrodes revealed relaxation processes of very different characteristic time scales, ranging from a 2 ms scale interface-normal ion transport, a 100 ms scale molecular reorientation, and a 60 s scale lateral ordering within the first layer [115, 116].

Adsorption of surfactants. Surfactant adsorption is often described by a two-step process: Diffusion towards the surface and the binding process [117, 118, 119, 120]. Usually, the first step is rate limiting. Thus, the minimal time required to form an adsorption layer is limited by diffusion [121, 122, 123, 124]. If the surface excess in equilibrium is denoted by Γ the relaxation time can be estimated with [117, 125]

$$\tau_{ad} = \frac{\pi}{4}\frac{\lambda^2}{D} = \frac{\pi}{4}\frac{\Gamma^2}{D c^2} \tag{15}$$

Here, λ is the depletion length, that is, the equivalent thickness of a layer in the liquid which contains the molecules required to reach a surface excess Γ. The depletion length $\lambda = \Gamma / c$ decreases with the concentration c. The diffusion coefficient D can again be related to the hydrodynamic radius of the molecule R by Eq. (13). Typical diffusion coefficients for common surfactants in water are D=2-5×10^{-10} m^2/s. For adsorption at the free water surface usually Γ=3-6 µmol/m^2 at the critical micellar concentration (CMC). As one example, we consider the non-ionic surfactant pentaethyleneglycol dodecyl ether ($C_{12}E_5$) [125] with a CMC of 0.065 mM. At a concentration equal to the CMC, the equilibrium value of the surface excess is 3.25×10^{-6} mol/m^2. With a diffusion coefficient of 4×10^{-10} m^2/s, the relaxation time for surfactant adsorption is τ_{ad}=4 s.

Formation of an electric double-layer. The electric potential of a charged surface in contact with an electrolyte solution decays roughly exponentially with distance. The characteristic

https://doi.org/10.1021/acs.langmuir.8b01783

decay length is the so-called Debye length. The Debye length for a monovalent salt solution is

$$\lambda_D = \sqrt{\frac{\varepsilon\varepsilon_0 k_B T}{2ce^2}} \tag{16}$$

Here, ε is the relative dielectric permittivity of the liquid, ε_0 = 8.85×10^{-12} AsV^{-1}m^{-1} is the vacuum permittivity, and e is the elementary charge. In most cases, the formation of such a double layer is limited by the diffusion of ions towards and away from the interface. The relaxation time associated with it can be estimated by the Debye time [126, 127, 128]

$$\tau_D = \frac{\lambda_D^2}{D_{salt}} \tag{17}$$

Here, D_{salt} is the diffusion coefficient for the salt, which can be calculated from $D_{salt} = 2D_+D_-/(D_+ + D_-)$, where D_+ and D_- are the diffusion coefficients of the cat- and anions. For a monovalent salt in water, typical diffusion coefficients are D_{salt}≈2.0×10^{-9} m^{2}s^{-1} leading to $\tau_D \approx$ 20 ns for 1 mM and 0.2 ns for 100 mM NaCl solution. The longest Debye lengths occur in distilled water at neutral pH. At pH 7 $\lambda_D \approx$ 1 µm so that with a mean diffusion coefficient of hydroxyl and hydronium ions of $D \approx$ 7×10^{-9} m^2/s we obtain τ_D = 130 µs. Practically, the pH is often around 6 due to absorbed carbon dioxide so that λ_D = 300 nm leading to a relaxation time around τ_D = 13 µs.

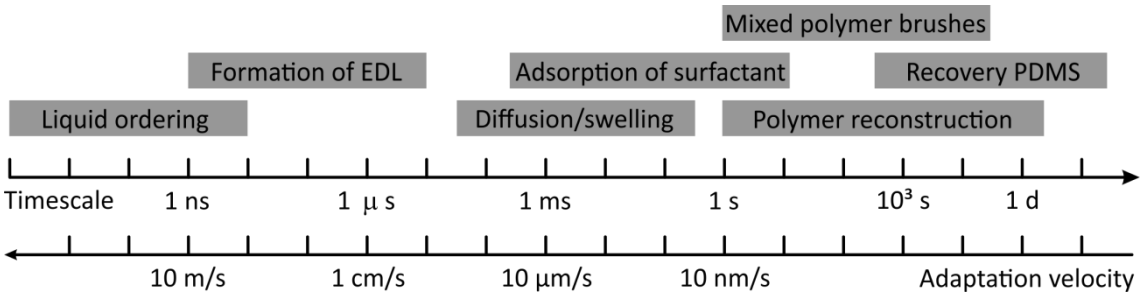

Figure 7. Time scales involved in adaptation processes of the solid and liquid side of the solid-liquid interface and of the free liquid surface. The corresponding adaptation velocities were estimated by dividing the peripheral thickness of 10 nm by the respective relaxation time.

Comparison with experiments

To compare the adaptation model with experimental results measurements of contact angles-versus-velocity on adaptive surfaces with known relaxation times are necessary. As a first step we fit known experimental results of Θ_a or Θ_r-vs-v to demonstrate that the model is quantitatively able to describe measured contact angles. Therefore, we fitted results of different experiments reported in the literature:

https://doi.org/10.1021/acs.langmuir.8b01783

- Vega et al. report advancing contact angles measured on a Nylon fiber which is immersed in water (η = 1.0 mPa s, γ_L^∞ = 72.8 mN/m), PDMS (η = 9.6 mPa s, γ_L^∞ = 19.6 mN/m), 60% aqueous glycerol solution (η = 35.0 mPa s, γ_L^∞ = 65.8 mN/m) and 66% thiodiglycerol in water (η = 10.8 mPa s, γ_L^∞ = 52.2 mN/m) [129]. Measured advancing contact angles could be fitted with $\Delta\gamma_{SL}$ in the range of 12-41 mN/m and adaptation velocities v_{SL} of 1-10 mm/s (Fig. 8A). Assuming a peripheral thickness of 10 nm an adaptation velocity of 1 to 10 mm/s leads to a relaxation time of 1-10 µs.
- A cylinder was coated with polystyrene, immersed horizontally with the axis into a water bath and rotated [130]. Results for receding contact angles for two different experiments are shown in Figure 8B. Receding contact angles could be fitted with $\Delta\gamma_{SL}$ = 18 mN/m and v_S = 1.0 mm/s.
- Ranabothu, Karnezis & Dai [131] measured dynamic contact angles on a glass plate covered with the fluoropolymer Teflon AF 1600 which was dipped into the liquid. They report advancing and receding contact angles for speeds up to 5 mm/s. Results could again be fitted with Eqs. (5) and (8). As examples, for water the fit leads to v_{SL} =0.1 mm/s and for formamide to v_{SL} =0.2 mm/s.
- Blake & Shikhmurzaev [77] use the plunging tape (PET) technique to measure the receding contact angle versus speed for water-glycerol mixtures. For velocities below a regime dominated by hydrodynamic forces, their contact angles could be fitted with $\Delta\gamma_{SL}$ = 9 mN/m and v_S = 0.03 mm/s for 16% glycerol (η = 1.5 mPa s, γ_L^∞ = 69.7 mN/m), $\Delta\gamma_{SL}$= 14 mN/m and v_S = 0.13 mm/s for 43% glycerol (η = 4.2 mPa s, γ_L^∞ = 64.9 mN/m) and $\Delta\gamma_{SL}$ = 26 mN/m and v_S = 0.1 mm/s for 95% glycerol (η = 672 mPa s, γ_L^∞ = 64.5 mN/m).

Thus, experimental results can be described by the adaptation model.

https://doi.org/10.1021/acs.langmuir.8b01783

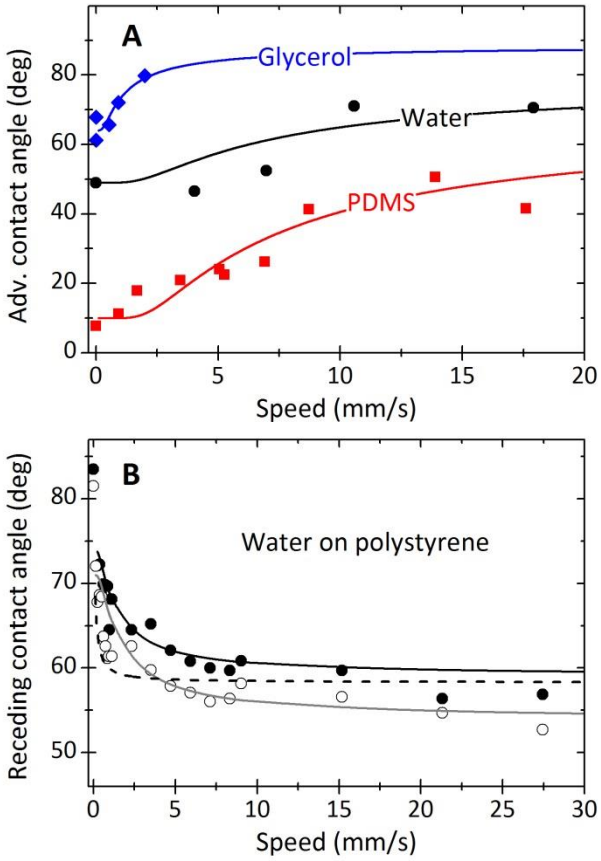

Figure 8. **(A)** Advancing contact angle on a Nylon fibre of 0.7 mm diameter measured with different liquids [129]. The experimental results were fitted with Eq. (5), obtaining the following parameters. Water: Θ^{∞} = 49°, $\Delta\gamma_{SL}$ = 33 mN/m, v_{SL} = 6.7 mm/s; PDMS: Θ^{∞} = 10°, $\Delta\gamma_{SL}$ = 12 mN/m, v_{SL} = 10 mm/s; glycerol solution: Θ^{∞} = 63°, $\Delta\gamma_{SL}$ = 27 mN/m, v_{SL} = 1 mm/s. **(B)** Receding contact angle measured with a rotating cylinder of 12 cm diameter coated with polystyrene (M_W=300 kg/mol) and half immersed in water [130]. Results of two different experiments are shown. The fitted curves (continuous lines) were fitted with Eq. (8) and Θ^{∞} = 74°, $\Delta\gamma_{SL}$ = 17.2 mN/m, v_S = 1.0 mm/s (top) and Θ^{∞} = 71°, $\Delta\gamma_{SL}$ = 19 mN/m, v_S = 1.2 mm/s (bottom). The dashed curve was calculated with Eq. (8) with Θ^{∞} = 74°, $\Delta\gamma_{SL}$ = 18 mN/m and v_S = 0.1 mm/s.

The fact that experimental results can be fitted with the adaptation model is a necessary but not sufficient condition that the model is correct. The same results could also be fitted with e.g. MKT theory [9, 132]. The main question is if the underlying physics is correct, that is, if an adaptation process takes place. Furthermore, the relation between the adaptation model and MKT theory or hydrodynamic modeling of dynamic contact angles needs investigation. Most likely, these questions will be difficult to answer with dynamic contact angle measurements alone. Predictions with MKT and the adaptation model are close to each other. To verify the adaptation approach for every single liquid-solid combination, the relaxation process needs to be identified and verified spectroscopically or microscopically.

https://doi.org/10.1021/acs.langmuir.8b01783

Adaptation combined with other effects leading to dynamic contact angles or contact angle hysteresis

Adaptation can take place simultaneously with other processes such as adsorption/ desorption or hydrodynamic dissipation. To consider multiple effects we combine predictions of MKT and hydrodynamic theory with the adaption theory. In MKT, the dependence of the dynamic contact angles on the velocity is described by [9]

$$v = 2K_0\lambda \cdot \sinh\left\{\frac{\gamma_L^\infty \lambda^2}{2k_B T}\left[\cos\Theta^\infty - \cos\Theta(v)\right]\right\} \qquad (18)$$

Here, K_0 as a quasi-equilibrium rate constant for adsorption/desorption of molecules and λ as the distance between adsorption sites. In Eq. (18) a positive velocity is in the forward direction. For the receding site a negative velocity needs to be inserted. To combine MKT with adaptation theory, we suggest replacing $\cos\Theta^\infty$ by $\cos\Theta_a$ from Eq. (5) for the dynamic advancing contact angle and with $\cos\Theta_r$ from Eq. (7) or (8) for the dynamic receding contact angle. The combined dynamic contact angles can then be obtained from calculating $\cos\Theta(v)$.

Hydrodynamic theory predicts

$$\Theta_a^3(v) = \Theta^{\infty 3} + \frac{9\eta v}{\gamma_L^\infty}\ln\frac{L_o}{L_i} \quad \text{and} \quad \Theta_r^3(v) = \Theta^{\infty 3} - \frac{9\eta v}{\gamma_L^\infty}\ln\frac{L_o}{L_i} \qquad (19)$$

for the advancing and receding dynamic contact angles [5, 6, 133]. Here, L_o is an outer, macroscopic length scale, for example the capillary length or the size of the drop. L_i represents an inner, microscopic, cutoff length scale, introduced to remove a singularity in the mathematical description [7]. To combine adaptation with hydrodynamic dissipation we follow Petrov & Petrov [134] and suggest to replace Θ^∞ in Eq. (19) by Θ_a from Eq. (5) or Θ_r from Eq. (7) to predict the dynamic advancing and receding contact angle, respectively.

Contact angle hysteresis is in practice often caused by multiple effects, such as heterogeneity or roughness. To calculate the adaptive advancing and receding contact angles it is tempting to replace Θ^∞ in Eq. (5) and (7) or (8) with the respective non-adapted advancing and receding contact angles. However, what may work for rough, homogeneous surfaces, will in general not work for heterogeneous surface. For heterogeneous surfaces the different components may adapt differently, leading to a specific and more complex change of contact angle hysteresis.

Conclusions

With the described model we quantitatively link adaptation processes to contact angle hysteresis and dynamic contact angle phenomena. Adaption can be on the solid or on the

https://doi.org/10.1021/acs.langmuir.8b01783

liquid side of the interface. The solid structure changes due to the presence of the liquid or its vapor. Also, the interfacial structure of the liquid can change depending if it is in contact with a solid or air. Adaptation results inherently in contact angle hysteresis. Moreover, adaptation directly causes a change in dynamic contact angles. To link dynamic advancing and receding contact angles to relaxation processes at interfaces, the peripheral thickness is introduced. The peripheral thickness is the width of the region on the surface which influences the contact angle. Dynamic contact angles vary around the adaptation velocity, which is the ratio of the peripheral thickness by the typical relaxation time of the adaptation process. Relevant questions to describe adaptive wetting are: What is the peripheral thickness? Which relaxation processes take place in a specific solid-liquid combination? What are their kinetics?

Acknowledgements

We acknowledge financial support from an ERC Grant No. 340391 SuPro (H.J.B.), the DFG SFB1194 C3 (H.J.B.), and the European Union's Horizon 2020 research and innovation program LubISS No 722497 (D.V.). Thanks to Abhinav Naga for editing the manuscript.

References

1. Bormashenko, E. Y. *Wetting of Real Surfaces*; De Gruyter2013; Vol. 19.
2. Ras, R. H. A.; Marmur, A. *Non-wettable Surfaces: Theory, Preparation and Applications*; Royal Society of Chemistry, 2017. p 391.
3. Starov, V. M.; Velarde, M. G.; Radke, C. J. *Wetting and Spreading Dynamics*; CRC Press: London, 2007. p 515.
4. Bonn, D.; Eggers, J.; Indekeu, J.; Meunier, J.; Rolley, E. Wetting and spreading. *Rev. Modern Physics* **2009,** *81*, 739-805.
5. Snoeijer, J. H.; Andreotti, B. Moving contact lines: Scales, regimes, and dynamical transitions. *Ann. Rev. Fluid Mech.* **2013,** *45*, 269-292.
6. Voinov, O. V. Hydrodynamics of wetting. *Fluid Dynamics* **1976,** *11*, 714-721.
7. Cox, R. G. The dynamics of the spreading of liquids on a solid surface. Part 1. Viscous flow. *J. Fluid Mech.* **1986,** *168*, 169-194.
8. Shikhmurzaev, Y. D. The moving contact line on a smooth solid surface. *Int. J. Multiphase Flow* **1993,** *19*, 589-610.
9. Blake, T. D. The physics of moving wetting lines. *J. Colloid Interface Sci.* **2006,** *299*, 1-13.
10. Luzinov, I.; Minko, S.; Tsukruk, V. V. Adaptive and responsive surfaces through controlled reorganization of interfacial polymer layers. *Prog. Polym. Sci.* **2004,** *29*, 635-698.

https://doi.org/10.1021/acs.langmuir.8b01783

11. Bryuzgin, E. V.; Hyakutake, T.; Navrotskiy, A. V.; Nishide, H.; Novakov, I. A. Control of surface wetting via production of graft polymer chains with adaptive behavior. *Protection of Metals and Physical Chemistry of Surfaces* **2013,** *49*, 101-108.
12. Cohen-Stuart, M. A.; Huck, W. T. S.; Genzer, J.; Muller, M.; Ober, C.; Stamm, M.; Sukhorukov, G. B.; Szleifer, I.; Tsukruk, V. V.; Urban, M.; Winnik, F.; Zauscher, S.; Luzinov, I.; Minko, S. Emerging applications of stimuli-responsive polymer materials. *Nature Materials* **2010,** *9*, 101-113.
13. Guo, F.; Guo, Z. G. Inspired smart materials with external stimuli responsive wettability: a review. *RSC Advances* **2016,** *6*, 36623-36641.
14. Lequeux, F.; Talini, L.; Verneuil, E.; Delannoy, G.; Valois, P. Wetting of polymers by their solvents. *Eur. Physical J. E* **2016,** *39*, 12.
15. Holly, F. J.; Refojo, M. F. Wettability of hydrogels. I. Poly(2-hydroxyethyl methacrylate). *J. Biomed. Mater. Res.* **1975,** *9*, 315-326.
16. Yasuda, H.; Sharma, A. K.; Yasuda, T. Effect of orientation and mobility of polymer molecules at surfaces on contact angle and its hysteresis. *J. Polym. Sci. Polym. Phys. Ed.* **1981,** *19*, 1285-1291.
17. Lavielle, L.; Schultz, J. Surface properties of graft polyethylene in contact with water. I. Orientation phenomena. *J. Colloid Interface Sci.* **1985,** *106*, 438-445.
18. Morra, M.; Occhiello, E.; Garbassi, F. Contact angle hysteresis on oxygen plasma treated polypropylene surfaces. *J. Colloid Interface Sci.* **1989,** *132*, 504-508.
19. Yasuda, T.; Okuno, T.; Yoshida, K.; Yasuda, H. A study of surface dynamics of polymers. II. Investigation by plasma surface implantation of fluorine-containing moieties. *J. Polymer Sci. B* **1988,** *26*, 1781-1794.
20. Yasuda, T.; Miyama, M.; Yasuda, H. Dynamics of the surface configuration change of polymers in response to changes in environmental conditions. 2. Comparison of changes in air and in liquid water. *Langmuir* **1992,** *8*, 1425-1430.
21. Sedev, R. V.; Budziak, C. J.; Petrov, J. G.; Neumann, A. W. Dynamic contact angles at low velocities. *J. Colloid Interface Sci.* **1993,** *159*, 392-399.
22. Wang, J. H.; Claesson, P. M.; Parker, J. L.; Yasuda, H. Dynamic contact angles and contact angle hysteresis of plasma polymers. *Langmuir* **1994,** *10*, 3887-3897.
23. Tretinnikov, O. N.; Ikada, Y. Dynamic wetting and contact angle hysteresis of polymer surfaces studied with the modified Wilhelmy balance method. *Langmuir* **1994,** *10*, 1606-1614.
24. Extrand, C. W.; Kumagai, Y. An experimental study of contact angle hysteresis. *J. Colloid Interface Sci.* **1997,** *191*, 378-383.
25. Crevoisier, G. B.; Fabre, P.; Corpart, J. M.; Leibler, L. Switchable tackiness and wettability of a liquid crystalline polymer. *Science* **1999,** *285*, 1246-1249.
26. Lam, C. N. C.; Wu, R.; Li, D.; Hair, M. L.; Neumann, A. W. Study of the advancing and receding contact angles: liquid sorption as a cause of contact angle hysteresis. *Adv. Colloid Interface Sci.* **2002,** *96*, 169-191.
27. Vaidya, A.; Chaudhury, M. K. Synthesis and surface properties of environmentally responsive segmented polyurethanes. *J. Colloid Interface Sci.* **2002,** *249*, 235–245.
28. Extrand, C. W. Water contact angles and hysteresis of polyamide surfaces. *J. Colloid Interface Sci.* **2002,** *248*, 136-142.

https://doi.org/10.1021/acs.langmuir.8b01783

29. Crowe, J. A.; Genzer, J. Creating responsive surfaces with tailored wettability switching kinetics and reconstruction reversibility. *J. Am. Chem. Soc.* **2005,** *127*, 17610-17611.
30. Tavana, H.; Neumann, A. W. On the question of rate-dependence of contact angles. *Colloids Surf. A* **2006,** *282*, 256-262.
31. Grundke, K.; Poschel, K.; Synytska, A.; Frenzel, R.; Drechsler, A.; Nitschke, M.; Cordeiro, A. L.; Uhlmann, P.; Welzel, P. B. Experimental studies of contact angle hysteresis phenomena on polymer surfaces - Toward the understanding and control of wettability for different applications. *Adv. Colloid Interface Sci.* **2015,** *222*, 350-76.
32. Fedors, R. F. Osmotiic effects in water adsorption by polymers. *Polymer* **1980,** *21*, 207-212.
33. Igarashi, S.; Itakura, A. N.; Toda, M.; Kitajima, M.; Chu, L.; Chifen, A. N.; Förch, R.; Berger, R. Swelling signals of polymer films measured by a combination of micromechanical cantilever sensor and surface plasmon resonance spectroscopy. *Sensors & Actuators B* **2006**, *117*, 43–49.
34. Liu, C. J.; Lopes, M. C.; Pihan, S. A.; Fell, D.; Sokuler, M.; Butt, H.-J.; Auernhammer, G. K.; Bonaccurso, E. Water diffusion in polymer nano-films measured with microcantilevers. *Sensors and Actuators B* **2011,** *160*, 32-38.
35. Lee, J. N.; Park, C.; Whitesides, G. M. Solvent compatibility of poly(dimethylsiloxane)-based microfluidic devices. *Analytical Chemistry* **2003,** *75*, 6544-6554.
36. Barrie, J. A.; Machin, D. The sorption and diffusion of water in silicone rubbers. 1. Unfilled rubbers. *J. Macromol. Sci. - Phys.* **1969,** *B3*, 645-672.
37. Watson, J. M.; Baron, M. G. The behaviour of water in poly(dimethylsiloxane). *J. Membrane Science* **1996,** *110*, 47-57.
38. Harley, S. J.; Glascoe, E. A.; Maxwell, R. S. Thermodynamic study on dynamic water vapor sorption in Sylgard-184. *J. Phys. Chem. B* **2012,** *116*, 14183-14190.
39. Zhang, R.; Graf, K.; Berger, R. Swelling of cross-linked polystyrene spheres in toluene vapor. *Appl. Phys. Lett.* **2006,** *89*, 223114.
40. Tokarev, I.; Minko, S. Stimuli-responsive hydrogel thin films. *Soft Matter* **2009,** *5*, 511-524.
41. Chen, L.; Liu, M. J.; Lin, L.; Zhang, T.; Ma, J.; Song, Y. L.; Jiang, L. Thermal-responsive hydrogel surface: tunable wettability and adhesion to oil at the water/solid interface. *Soft Matter* **2010,** *6*, 2708-2712.
42. Yoon, J. W.; Cai, S. Q.; Suo, Z. G.; Hayward, R. C. Poroelastic swelling kinetics of thin hydrogel layers: comparison of theory and experiment. *Soft Matter* **2010,** *6*, 6004-6012.
43. Gharekhani, H.; Olad, A.; Mirmohseni, A.; Bybordi, A. Superabsorbent hydrogel made of NaAlg-g-poly(AA-co-AAm) and rice husk ash: Synthesis, characterization, and swelling kinetic studies. *Carbohydrate Polymers* **2017,** *168*, 1-13.
44. Zhang, H.; Gao, X.; Chen, K. L.; Li, H.; Peng, L. C. Thermo-sensitive and swelling properties of cellouronic acid sodium/poly (acrylamide-co-diallyldimethylammonium chloride) semi-IPN. *Carbohydrate Polymers* **2018,** *181*, 450-459.

https://doi.org/10.1021/acs.langmuir.8b01783

45. Karadag, E.; Üzüm, O. B.; Saraydin, D.; Güven, O. Dynamic swelling behavior of gamma-radiation induced polyelectrolyte poly(AAm-co-CA) hydrogels in urea solutions. *Int. J. Pharm.* **2005,** *301*, 102-111.
46. Minko, S.; Müller, M.; Usov, D.; Scholl, A.; Froeck, C.; Stamm, M. Lateral versus perpendicular segregation in mixed polymer brushes. *Phys. Rev. Lett.* **2002,** *88*, 035502.
47. Minko, S.; Müller, M.; Motornov, M.; Nitschke, M.; Grundke, K.; Stamm, M. Two-level structured self-adaptive surfaces with reversibly tunable properties. *J. Am. Chem. Soc.* **2003,** *125*, 3896-3900.
48. Zhao, B.; He, T. Synthesis of well-defined mixed poly(methyl methacrylate)/ polystyrene brushes from an asymmetric difunctional initiator-terminated self-assembled monolayer. *Macromolecules* **2003,** *36*, 8599-8602.
49. Edmondson, S.; Osborne, V. L.; Huck, W. T. S. Polymer brushes via surface-initiated polymerizations. *Chem. Soc. Rev.* **2004,** *33*, 14-22.
50. Lupitskyy, R.; Roiter, Y.; Tsitsilianis, C.; Minko, S. From smart polymer molecules to responsive nanostructured surfaces. *Langmuir* **2005,** *21*, 8591-8593.
51. Li, D.; Sheng, X.; Zhao, B. Environmentally responsive "hairy" nanoparticles: Mixed homopolymer brushes on silica nanoparticles synthesized by living radical polymerization techniques. *J. Am. Chem. Soc.* **2005,** *127*, 6248-6256.
52. Santer, S.; Kopyshev, A.; Yang, H. K.; Rühe, J. Local composition of nanophase-separated mixed polymer brushes. *Macromolecules* **2006,** *29*, 3056-3064.
53. Sui, X.; Zapotoczny, S.; Benetti, E. M.; Memesa, M.; Hempeniusa, M. A.; Vancso, G. J. Grafting mixed responsive brushes of poly(N-isopropylacrylamide) and poly(methacrylic acid) from gold by selective initiation. *Polym. Chem.* **2011,** *2*, 879-884.
54. Tonhauser, C.; Golriz, A. A.; Moers, C.; Klein, R.; Butt, H.-J.; Frey, H. Stimuli-responsive Y-shaped polymer brushes based on junction-point-reactive block copolymers. *Adv. Mater.* **2012,** *24*, 5559-5563.
55. Ionov, L.; Minko, S. Mixed polymer brushes with locking switching. *ACS Appl. Materials & Interfaces* **2012,** *4*, 483-489.
56. Ochsmann, J. W.; Lenz, S.; Lellig, P.; Emmerling, S. G. J.; Golriz, A. A.; Reichert, P.; You, J. C.; Perlich, J.; Roth, S. V.; Berger, R.; Gutmann, J. S. Stress-structure correlation in PS-PMMA mixed polymer brushes. *Macromolecules* **2012,** *45*, 3129-3136.
57. Morra, M.; Occhiello, E.; Marola, R.; Garbassi, F.; Humphrey, P.; Johnson, D. On the aging of oxygen plasma-treated polydimethylsiloxane surfaces. *J. Colloid Interface Sci.* **1990,** *137*, 11-24.
58. Gubanski, S. M.; Vlastós, A. E. Wettability of naturally aged silicone and EPDM composite insulators. *IEEE Transactions on Power Delivery* **1990,** *5*, 1527-1535.
59. Fritz, J. L.; Owen, M. J. Hydrophobic recovery of plasma-treated polydimethylsiloxane. *J. Adhesion* **1995,** *54*, 33-45.
60. Dupont-Gillain, C. C.; Adriaensen, Y.; Derclaye, S.; Rouxhet, P. G. Plasma-oxidized polystyrene: Wetting properties and surface reconstruction. *Langmuir* **2000,** *16*, 8194-8200.

https://doi.org/10.1021/acs.langmuir.8b01783

61. Hillborg, H.; Tomczak, N.; Olah, A.; Schönherr, H.; Vancso, G. J. Nanoscale hydrophobic recovery: A chemical force microscopy study of UV/ozone-treated cross-linked poly(dimethylsiloxane). *Langmuir* **2004,** *20*, 785-794.

62. Kim, J.; Chaudhury, M. K.; Owen, M. J. Modeling hydrophobic recovery of electrically discharged polydimethylsiloxane elastomers. *J. Colloid Interface Sci.* **2006,** *293*, 364–375.

63. Inutsuka, M.; Yamada, N. L.; Ito, K.; Yokoyama, H. High density polymer brush spontaneously formed by the segregation of amphiphilic diblock copolymers to the polymer/water interface. *ACS Macro Lett.* **2013,** *2*, 265-268.

64. Inutsuka, M.; Tanoue, H.; Yamada, N. L.; Ito, K.; Yokoyama, H. Dynamic contact angle on a reconstructive polymer surface by segregation. *RSC Advances* **2017,** *7*, 17202-17207.

65. Yu, X.; Wang, Z. Q.; Jiang, Y. G.; Shi, F.; Zhang, X. Reversible pH-responsive surface: From superhydrophobicity to superhydrophilicity. *Adv. Mater.* **2005,** *17*, 1289-1293.

66. Moreno Flores, S.; Shaporenko, A.; Vavilala, C.; Butt, H.-J.; Schmittel, M.; Zharnikov, M.; Berger, R. Control of surface properties of self-assembled monolayers by fine-tuning the degree of molecular asymmetry. *Surf. Sci.* **2006,** *206*, 2847-2856.

67. Cheng, M. J.; Liu, Q.; Ju, G. N.; Zhang, Y. J.; Jiang, L.; Shi, F. Bell-shaped superhydrophilic-superhydrophobic-superhydrophilic double transformation on a pH-responsive smart surface. *Adv. Mater.* **2014,** *26*, 306-310.

68. Allara, D. L.; Parikh, A. N.; Judge, E. The existence of structure progressions and wetting transitions in intermediately disordered monolayer alkyl chain assemblies. *J. Chem. Phys.* **1994,** *100*, 1761-1764.

69. Kacker, N.; Kumar, S. K.; Allara, D. L. Wetting-induced reconstruction in molecular surfaces. *Langmuir* **1997,** *13*, 6366-6369.

70. Bartell, F. E.; Cardwell, P. H. Reproducible contact angles on reproducible metal surfaces. 1. Contact angles of water against silver and gold. *J. Am. Chem. Soc.* **1942,** *64*, 494-497.

71. Schrader, M. E. Wettability of clean metal surfaces. *J. Colloid Interface Sci.* **1984,** *100*, 372-380.

72. Israelachvili, J. N.; Alcantar, N. A.; Maeda, N.; Mates, T. E.; Ruths, M. Preparing contamination-free mica substrates for surface characterization, force measurements, and imaging. *Langmuir* **2004,** *20*, 3616-3622.

73. Li, Z. T.; Kozbial, A.; Nioradze, N.; Parobek, D.; Shenoy, G. J.; Salim, M.; Amemiya, S.; Li, L.; Liu, H. T. Water protects graphitic surface from airborne hydrocarbon contamination. *ACS Nano* **2016,** *10*, 349-359.

74. Forrest, E.; Schulze, R.; Liu, C.; Dombrowski, D. Influence of surface contamination on the wettability of heat transfer surfaces. *Intl. J. Heat Mass Transfer* **2015,** *91*, 311-317.

75. Hansen, R. S.; Miotto, M. Relaxation phenomena and contact angle hysteresis. *J. Am. Chem. Soc.* **1957,** *79*, 1765-1765.

76. Elliott, G. E. P.; Riddiford, A. C. Dynamic contact angles.1. Effect of impressed motion. *J. Colloid Interface Sci.* **1967,** *23*, 389-398.

https://doi.org/10.1021/acs.langmuir.8b01783

77. Blake, T. D.; Shikhmurzaev, Y. D. Dynamic wetting by liquids of different viscosity. *J. Colloid Interface Sci.* **2002,** *253*, 196-202.
78. Lee, K. S.; Ivanova, N.; Starov, V. M.; Hilal, N.; Dutschk, V. Kinetics of wetting and spreading by aqueous surfactant solutions. *Adv. Colloid Interface Sci.* **2008,** *144*, 54-65.
79. Starov, V. M.; Kosvintsev, S. R.; Velarde, M. G. Spreading of surfactant solutions over hydrophobic substrates. *J. Colloid Interface Sci.* **2000,** *227*, 185-190.
80. Luokkala, B. B.; Garoff, S.; Tilton, R. D.; Suter, R. M. Interfacial structure and rearrangement of nonionic surfactants near a moving contact line. *Langmuir* **2001,** *17*, 5917-5923.
81. Furmidge, C. G. L. Studies at phase interfaces. I. The sliding of liquid drops on solid surfaces and a theory for spray retention. *J. Colloid Sci.* **1962,** *17*, 309-324.
82. Yoshimitsu, Z.; Nakajima, A.; Watanabe, T.; Hashimoto, K. Effects of surface structure on the hydrophobicity and sliding behavior of water droplets. *Langmuir* **2002,** *18*, 5818-5822.
83. ElSherbini, A.; Jacobi, A. Retention forces and contact angles for critical liquid drops on non-horizontal surfaces. *J. Colloid Interface Sci.* **2006,** *299*, 841-849.
84. Antonini, C.; Carmona, F. J.; Pierce, E.; Marengo, M.; Amirfazli, A. General methodology for evaluating the adhesion force of drops and bubbles on solid surfaces. *Langmuir* **2009,** *25*, 6143-6154.
85. Eral, H. B.; t'Mannetje, D. J. C. M.; Oh, J. M. Contact angle hysteresis: a review of fundamentals and applications. *Colloid Polymer Sci.* **2013,** *291*, 247-260.
86. Timonen, J. V. I.; Latikka, M.; Ikkala, O.; Ras, R. H. A. Free-decay and resonant methods for investigating the fundamental limit of superhydrophobicity. *Nature commun.* **2013,** *4*, 2398.
87. Gao, N.; Geyer, F.; Pilat, D. W.; Wooh, S.; Vollmer, D.; Butt, H.-J.; Berger, R. How drops start sliding over solid surfaces. *Nature Physics* **2017,** *14*, 191.
88. Cain, J. B.; Francis, D. W.; Venter, R. D.; Neumann, A. W. Dynamic contact angles on smooth and rough surfaces. *J. Colloid Interface Sci.* **1983,** *94*, 123-130.
89. Hardy, W. B. The spreading of fluids on glass. *Phil. Mag.* **1919,** *38*, 49-55.
90. Zisman, W. A. Relation of the equilibrium contact angle to liquid and solid constitution. *Advances in Chemistry Series* **1964,** *43*, 1-51.
91. Frank, B.; Garoff, S. Surfactant self-assembly near contact lines: Control of advancing surfactant solutions. *Colloids Surfaces A* **1996,** *116*, 31-42.
92. Churaev, N. V.; Starov, V. M.; Derjaguin, B. V. The shape of the transition zone between a thin film and bulk liquid and the line tension. *J. Colloid Interface Sci.* **1982,** *89*, 16-24.
93. de Gennes, P. G. Wetting: Statics and dynamics. *Rev. Modern Phys.* **1985,** *57*, 827-863.
94. Deryaguin, B. V.; Starov, V. M.; Churaev, N. V. Profile of the transition zone between a wetting film and the meniscus of the bulk liquid. *Kolloidn. Zh.* **1976,** *38*, 875-879.
95. Pericet-Camara, R.; Best, A.; Butt, H.-J.; Bonaccurso, E. Effect of capillary pressure and surface tension on the deformation of elastic surfaces by sessile liquid microdrops: An experimental investigation. *Langmuir* **2008,** *24*, 10565-10568.

https://doi.org/10.1021/acs.langmuir.8b01783

96. Marchand, A.; Das, S.; Snoeijer, J. H.; Andreotti, B. Capillary pressure and contact line force on a soft solid. *Phys. Rev. Lett.* **2012,** *108*, 094301.

97. Seveno, D.; Blake, T. D.; De Coninck, J. Young's equation at the nanoscale. *Phys. Rev. Lett.* **2013,** *111*, 096101.

98. Fernandez-Toledano, J. C.; Blake, T. D.; Lambert, P.; De Coninck, J. On the cohesion of fluids and their adhesion to solids: Young's equation at the atomic scale. *Adv. Colloid Interface Sci.* **2017,** *245*, 102-107.

99. Monson, L.; Braunwarth, M.; Extrand, C. W. Moisture absorption by various polyamides and their associated dimensional changes. *J. Appl. Polymer Sci.* **2008,** *107*, 355–363.

100. Tanaka, T.; Fillmore, D. J. Kinetics of swelling gels. *J. Chem. Phys.* **1979,** *70*, 1214-1218.

101. Li, Y.; Tanaka, T. Kinetics of swelling and shrinking of gels. *J. Chem. Phys.* **1990,** *92*, 1365-1371.

102. Schott, H. Kinetics of swelling of polymers and their gels. *J. Pharmaceutical Sci.* **1992,** *81*, 467-470.

103. Hong, W.; Zhao, X. H.; Zhou, J. X.; Suo, Z. G. A theory of coupled diffusion and large deformation in polymeric gels. *J. Mech. Phys. Solids* **2008,** *56*, 1779-1793.

104. Garcia, D. M.; Escobar, J. L.; Bada, N.; Casquero, J.; Hernaez, E.; Katime, I. Synthesis and characterization of poly(methacrylic acid) hydrogels for metoclopramide delivery. *Europ. Polymer J.* **2004,** *40*, 1637-1643.

105. Julthongpiput, D.; Lin, Y. S.; Teng, J.; Zubarev, E. R.; Tsukruk, V. V. Y-shaped polymer brushes: Nanoscale switchable surfaces. *Langmuir* **2003,** *19*, 7832-7836.

106. LeMieux, M. C.; Julthongpiput, D.; Bergman, K. N.; Cuong, P. D.; Ahn, H. S.; Lin, Y. H.; Tsukruk, V. V. Ultrathin binary grafted polymer layers with switchable morphology. *Langmuir* **2004,** *20*, 10046-10054.

107. Blackmore, P.; Birtwhistle, D. Surface discharges on polymeric insulator shed surfaces. *IEEE Transactions on Dielectrics and Electrical Insulation* **1997,** *4*, 210-217.

108. Tanoue, H.; Inutsuka, M.; Yamada, N. L.; Ito, K.; Yokoyama, H. Kinetics of dynamic polymer brush formation. *Macromolecules* **2017,** *50*, 5549-5555.

109. Hsieh, C. S.; Campen, R. K.; Verde, A. C. V.; Bolhuis, P.; Nienhuys, H. K.; Bonn, M. Ultrafast reorientation of dangling OH groups at the air-water interface using femtosecond vibrational spectroscopy. *Phys. Rev. Lett.* **2011,** *107*, 116102.

110. Fayer, M. D. Dynamics of water interacting with interfaces, molecules, and ions. *Acc. Chem. Research* **2012,** *45*, 3-14.

111. Xiao, S. H.; Figge, F.; Stirnemann, G.; Laage, D.; McGuire, J. A. Orientational dynamics of water at an extended hydrophobic interface. *J. Am. Chem. Soc.* **2016,** *138*, 5551-5560.

112. Bonn, M.; Nagata, Y.; Backus, E. H. G. Molecular structure and dynamics of water at the water-air interface studied with surface-specific vibrational spectroscopy. *Angew. Chem. Int. Ed.* **2015,** *54*, 5560-5576.

113. Benjamin, I. Static and dynamic electronic spectroscopy at liquid interfaces. *Chem. Rev.* **2006,** *106*, 1212-1233.

https://doi.org/10.1021/acs.langmuir.8b01783

114. Karnes, J. J.; Gobrogge, E. A.; Walker, R. A.; Benjamin, I. Unusual structure and dynamics at silica/methanol and silica/ethanol interfaces - A molecular dynamics and nonlinear optical study. *J. Phys. Chem. B* **2016,** *120*, 1569-1578.

115. Rotenberg, B.; Salanne, M. Structural transitions at ionic liquid interfaces. *J. Phys. Chem. Lett.* **2015,** *6*, 4978-4985.

116. Reichert, P.; Kjaer, K. S.; van Driel, T. B.; Mars, J.; Ochsmann, J. W.; Pontoni, D.; Deutsch, M.; Nielsen, M. M.; Mezger, M. Molecular scale structure and dynamics at an ionic liquid/electrode interface. *Faraday Discussions* **2018,** *206*, 141-157.

117. Ward, A. F. H.; Tordai, L. Time-dependence of boundary tensions of solutions. *J. Chem. Phys.* **1946,** *14*, 453-461.

118. Paria, S.; Khilar, K. C. A review on experimental studies of surfactant adsorption at the hydrophilic solid-water interface. *Adv. Colloid Interface Sci.* **2004,** *110*, 75-95.

119. Kanokkarn, P.; Shiina, T.; Santikunaporn, M.; Chavadej, S. Equilibrium and dynamic surface tension in relation to diffusivity and foaming properties: Effects of surfactant type and structure. *Colloids & Surfaces A* **2017,** *524*, 135-142.

120. Fainerman, V. B.; Miller, R. Dynamic surface tension measurements in the sub-millisecond range. *J. Colloid Interface Sci.* **1995,** *175*, 118-121.

121. Kairaliyeva, T.; Aksenenko, E. V.; Mucic, N.; Makievski, A. V.; Fainerman, V. B.; Miller, R. Surface tension and adsorption studies by drop profile analysis tensiometry. *J. Surfact. Deterg.* **2017,** *20*, 1225-1241.

122. Miller, R.; Aksenenko, E. V.; Fainerman, V. B. Dynamic interfacial tension of surfactant solutions. *Adv. Colloid Interface Sci.* **2017,** *247*, 115-129.

123. Svitova, T. F.; Wetherbee, M. J.; Radke, C. J. Dynamics of surfactant sorption at the air/water interface: continuous-flow tensiometry. *J. Colloid Interface Sci.* **2003,** *261*, 170-179.

124. Stückrad, B.; Hiller, W. J.; Kowalewski, T. A. Measurement of dynamic surface tension by the oscillating droplet method. *Experiments in Fluids* **1993,** *15*, 332-340.

125. Taylor, C. D.; Valkovska, D. S.; Bain, C. D. A simple and rapid method for the determination of the surface equations of state and adsorption isotherms for efficient surfactants. *Phys. Chem. Chem. Phys.* **2003,** *5*, 4885-4891.

126. Hunter, R. J. *Foundations of Colloid Science II*; Clarendon Press: Oxford, 1995; Vol. 2.

127. O'Brien, R. W. The high-frequency dielectric dispersion of a colloid. *J. Coll. Interf. Sci.* **1986,** *113*, 81-93.

128. Collins, L.; Jesse, S.; Kilpatrick, J. I.; Tselev, A.; Varenyk, O.; Okatan, M. B.; Weber, S. A. L.; Kumar, A.; Balke, N.; Kalinin, S. V.; Rodriguez, B. J. Probing charge screening dynamics and electrochemical processes at the solid-liquid interface with electrochemical force microscopy. *Nature Commun.* **2014,** *5*, 3871.

129. Vega, M. J.; Gouttiere, C.; Seveno, D.; Blake, T. D.; Voue, M.; de Coninck, J. Experimental investigation of the link between static and dynamic wetting by forced wetting of nylon filament. *Langmuir* **2007,** *23*, 10628-10634.

130. Henrich, F.; Fell, D.; Truszkowska, D.; Weirich, M.; Anyfantakis, M.; Nguyen, T. H.; Wagner, M.; Auernhammer, G. K.; Butt, H. J. Influence of surfactants in forced dynamic dewetting. *Soft Matter* **2016,** *12*, 7782-7791.

131. Ranabothu, S. R.; Karnezis, C.; Dai, L. L. Dynamic wetting: Hydrodynamic or molecular-kinetic? *J. Colloid Interface Sci.* **2005,** *288*, 213-221.

132. Blake, T. D.; Haynes, J. M. Kinetics of liquid/liquid displacement. *J. Colloid Interface Sci.* **1969,** *30*, 421-423.

133. Eggers, J. Hydrodynamic theory of forced dewetting. *Phys. Rev. Lett.* **2004,** *93*, 094502.

134. Petrov, P. G.; Petrov, J. G. A combined molecular-hydrodynamic appraoch to wetting kinetics. *Langmuir* **1992,** *8*, 1762-1767.

https://doi.org/10.1021/acs.langmuir.8b01783

TOC Figure